Computational Design of Nanobody Binding to Cortisol to Improve Their Binding Affinity Using Molecular Docking and Molecular Dynamics Simulations

Umi Baroroh[1*], Nur Asni Setiani[1], Irma Mardiah[1], Dewi Astriany[2], and Muhammad Yusuf[3,4]

[1]*Department of Biotechnology Pharmacy, Indonesian School of Pharmacy, Bandung, 40266, West Java, Indonesia*

[2]*Department of Pharmacy, Indonesian School of Pharmacy, Bandung, 40266, West Java, Indonesia*

[3]*Department of Chemistry, Faculty of Mathematics and Natural Sciences, Universitas Padjadjaran, Sumedang, 45363, West Java, Indonesia*

[4]*Research Center for Molecular Biotechnology and Bioinformatics, Jl. Singaperbangsa No. 2, Bandung 40133, West Java, Indonesia*

Abstract: *Currently, nanobody binding cortisol has been deposited in the database. Unfortunately, the affinity is still in micromolar order. Substituting hydrophobic residues in the binding pocket and utilizing CDR2 and CDR3 is the strategy to improve the affinity. A single and double substitution at positions 53 and 101 have been introduced to the nanobody structure through molecular modeling. The affinity toward cortisol was evaluated using molecular docking to get the binding pose. The highest binding energy pose was used as the initial coordinate to analyze further using 100 ns molecular dynamics simulations. The binding affinities calculated by MMGBSA showed that MT3, MT5, and MT6 have better binding affinity than WT. In contrast, the ligand movement through MD simulations reveals that MT1, MT3, and MT5 are relatively stable. Hence, docking and MD simulations showed that MT3 is the best mutant than others. This mutant is substituting the threonine to isoleucine at position 53. New hydrophobic interactions occurred and caused the increase of binding. Eventually, this study provides valuable structural information to improve the binding affinity of nanobody binding cortisol for further development of this molecule to antibody-based biosensor design.*

Keywords: *nanobody; cortisol; molecular dynamics simulations; molecular docking*

■ INTRODUCTION

Antibodies play a crucial role in the immune system. The molecule produced by B lymphocytes recognizes the foreign biological or chemical substance in high specificity [1]. They have a high affinity and selectivity for a molecule with low molecular weight (hapten) [2-3]. Antibodies are widely used in various applications, including diagnostic, therapy, and research. Unfortunately, their significant molecular weight (MW: 150,000 g/mol) and the high total number of disulfide bonds make them challenging to produce in bacteria or eukaryotic cells' cytoplasm [4-5]. The small molecule of the single-chain variable fragment (scFv), which consists of the variable domain of the heavy and light polypeptide chains joined together with a synthetic linker to form a single polypeptide chain, has several advantages. For example, bacteria can produce it because of its low molecular weight (MW: 30,000 g/mol). However, their fragile behavior leading to denaturation or aggregation or a spontaneous dimerization into diabodies remains an obvious flaw that complicates further application [6].

Fortunately, *Camelidae* family members (e.g., camels, llamas, and alpaca) have a subset of IgG antibodies that lack light chains, resulting in antibodies with only a single variable domain, VHH, that bind target molecules. This nanometer-sized antibody, approximately 2.5 nm in diameter and 4.2 nm in length, is called nanobodies (Nb) [7]. Aside from its small molecular size, some advantages include resistance to organic solvent, high solubility, and ease of production

in bacteria as a recombinant protein. This molecule is widely used in basic life science research, drug discovery, cancer diagnosis and treatment, and neurodegenerative and infectious diseases [8]. Some VHH bound to haptens have been reported to date: Spinelli et al. [9] determined the complex structure of azo-dye bound by VHH antibody; Fanning et al. [3] determined the structure of nanobodies attached to methotrexate (MTX); Rosa et al. [2] determined the structure of nanobodies bound to triclocarban (TCC), and Ding et al. [10] determined the structure of nanobodies attached to cortisol.

Cortisol, a steroid hormone, is a biomarker for some diseases and is essential in regulating psychological processes such as blood pressure, glucose levels, and carbohydrate metabolism [11]. Cortisol deficiency can result in Addison's disease. On the other hand, a persistent cortisol excess can result in Cushing's syndrome, leading to severe fatigue, depression, anxiety, cognitive difficulties, obesity, and cardiovascular disease [12-13]. Cortisol is commonly referred to as the "stress hormone" because of its fluctuating levels [14]. Continuous monitoring of cortisol levels is essential to preserve good health. Lately, cortisol measurements have been developed to determine whether variations in cortisol levels can be used as precursors for medically and psychologically relevant events like stress and, more recently, post-traumatic stress disorder (PTSD) [15-16].

Total cortisol is currently defined as the sum of the free cortisol and the protein-bound fraction. However, free cortisol is the only biologically active fraction [17-18] and is responsible for all cortisol-related activities in the body. As a result, regular estimation of free cortisol is required for accurate diagnosis and treatment. For the most part, current strategies are still limited to laboratory techniques such as chromatography, immunoassay, or electrochemical immuno-sensing [19] that are laborious, time-consuming, require large sample sizes, are expensive, and cannot be implemented as rapid test kits [20-21]. However, because of its high stability and tolerance to highly concentrated organic solvents, VHH antibodies can displace fragile traditional IgG antibodies in an ELISA and chip-based micro-detection system. Ding et al. determined the crystal structure of the VHH

complex with cortisol [10]. Cortisol mainly binds to the CDR1 of the VHH antibody. The interaction occurred in forming a hydrophobic pocket into which the majority of the hydrophobic portion of cortisol molecule inserted itself. Unfortunately, the binding affinity was not sufficiently high.

Therefore, we designed new mutants to improve the binding affinity by replacing amino acids at CDR2 and CDR3 with hydrophobic amino acids in the present study. The binding affinity was addressed using molecular docking and molecular dynamics (MD) simulations. It is hoped that the results will aid in developing Nb with a higher affinity to cortisol for diagnostic purposes.

■ COMPUTATIONAL METHODS

Modeling of Mutants

All mutants were built using the comparative modeling method using MODELLER 9.19 [22]. As a starting point, the structure of Nb-Cor (PDB ID: 6ITP) was used as a modeling template. The selection of the template is an essential step in comparative modeling. The quality of the template's structure is 1.57 Å resolution, and the quality of mutants was assessed using the Discrete Optimized Protein Energy (DOPE) score, Ramachandran plot, and Z-score. All mutants were designed based on the initial interaction observed in WT and substituted hydrophobic amino acids at residue numbers 53 and 101. All mutants are listed in Table 1.

Molecular Docking

The structure of Nb and its mutants were prepared using BIOVIA Discovery Studio 2017 Visualizer by separating the cortisol ligand, discarding the water molecules, and completing the structure by adding

Table 1. List of mutants

No.	Mutant	Description
1	MT1	T53V
2	MT2	T53L
3	MT3	T53I
4	MT4	S101V
5	MT5	T53V/S101V
6	MT6	T53L/S101V

hydrogen atoms. AutoDockTools-1.5.6 was used to convert all structures into PDBQT format. The crystal structure of Nb-Cor (PDB ID 6ITP) was redocked to validate the molecular docking method. The grid box size of $50 \times 50 \times 50$ points with a spacing of 0.375 Å was placed in the center of the Nb binding site. The pre-calculated binding affinity of the ligand's atom type was prepared using Autogrid [23].

AutoDock program is responsible for conformational search and energy evaluation. The Lamarckian Genetic Algorithm (LGA) parameter was set at 100 runs, elitism of 1, the mutation rate of 0.02, the population size of 150, a crossover rate of 0.800, and energy evaluation of 2,500,000 [24]. The resulting docked conformations were clustered using a root-mean-square deviation (RMSD) tolerance of 1.0 Å. The ligand conformational with the lowest free energy of binding (ΔG) was selected for further MD simulations.

Molecular Dynamics Simulations

The ligand conformational obtained from molecular docking was used as an initial coordinate. MD simulations were used to evaluate the binding of cortisol. MD simulations were carried out on a computer running Ubuntu 20.04.2.0 LTS and equipped with an Intel Xeon ® CPU E5-2678 v3 @2.5 GHz × 24, a GPU NVIDIA Ge Force RTX 2080Ti 6 GB, and 16 GB of RAM. The MD simulations procedure was adapted from our prior research [25]. In brief, the ligand (cortisol) parameter was calculated using the AM1-BCC approach by antechamber program [26]. The other parameter was calculated using Generalized Amber Force Fields 2 (GAFF2) [27], while FF19SB was assigned to Nb and its mutants' amino acid residues. All complex system was prepared using tleap program in AmberTools20. The solvent system of a box TIP3P water was added to the solute with the shortest distance of 10 Å between the protein and the box edge. To neutralize the system, the chloride ion was added. GPU-accelerated Particle-Mesh Ewald Molecular Dynamics (PMEMD) and periodic boundary conditions, as implemented in Amber20, were applied for each protein-ligand complex. Initially, energy minimization was implemented in three stages. First, 1,000 steps of the steepest gradient algorithm followed by 2,000 steps of conjugate gradient minimization with a harmonic restraint of 500 kcal/mol Å^2 were applied to the backbone atoms. A final 1,000 steps of unrestrained conjugate gradient minimization were performed to remove any sterically clashes among the atoms.

The system was gradually heated to room temperature (298 K) over 60 ns in the NVT ensemble. In this stage, a harmonic restraint of 5 kcal/mol Å^2 on the complex was applied to the complex. In addition, 1 ns of NPT equilibration was conducted. Harmonic restraint is gradually reduced by 1 kcal/mol Å^2 at this stage until it reaches zero. The production stage was run in the NPT ensemble for 100 ns. The time step at the production run was 2 fs since the SHAKE algorithm was used. Langevin thermostat was used to control the temperature. The collision frequency was set to 1 ps^{-1}. The pressure was controlled using a Berendsen barostat. The coupling constant parameter and target pressure were set to 1 ps and 1 bar, respectively. The nonbonded cutoff value was set to 9 Å. Particle Mesh Ewald was activated to treat the long-range electrostatics.

Trajectory Analysis

We utilized the *cpptraj* program in AmberTools20 to analyze MD trajectories. The analysis includes computation of Root-Mean-Square Fluctuation (RMSF), Root-Mean-Square Deviation (RMSD), and H-bond conservation.

Binding Energy Calculation

We used the MMPBSA.py program to calculate the pairwise interaction energy using a single trajectory method [28]. Binding free energy (ΔG$_{bind}$) between nanobody and cortisol was calculated based on MM/GBSA method:

$$\Delta G_{bind} = \Delta H - T\Delta S \approx \Delta E_{MM} + \Delta G_{sol} - T\Delta S$$
$$\Delta E_{MM} = \Delta E_{internal} + \Delta E_{electrostatic} + \Delta E_{vdw}$$
$$\Delta G_{sol} = \Delta G_{GB} + \Delta G_{SA}$$

In these equations, ΔH denotes enthalpy, and T denotes temperature (K). ΔE$_{MM}$ is the molecular mechanical (MM) energy change in the gas phase, which comprises of ΔE$_{internal}$ (internal energy), ΔE$_{electrostatic}$ (Coulomb electrostatics term), and ΔE$_{vdw}$ (van der Waals

interaction term). ΔG_{sol} is the solvation free energy, consists of ΔG_{GB} (electrostatic solvation energy or polar contribution calculated by GB method) and ΔG_{SA} (non-electrostatic solvation component or nonpolar contribution). The interval step and salt concentrations were 1 ns and 150 mM in the binding energy calculation, respectively.

■ RESULTS AND DISCUSSION

Nanobody, which are small antibody derivatives made up of only the heavy chains of camelid antibodies, have a wide range of applications, including diagnostic, therapeutic, and research [1]. Nb can be designed to have a high binding affinity to cortisol to diagnose cortisol. Based on the initial non-bonding interaction in the crystal structure, hydrophobic interaction between V24 and W34 to the cortisol in CDR1 occurred (Fig. 1). To improve the binding affinity of cortisol, other CDR should be utilized by modifying the amino acid to interact with cortisol. The anti-MTX-VHH was modified by introducing five residues from the original CDR4 loop into the CDR1-3 graft, resulting in a 1,000-fold increase in affinity. The non-hypervariable loop of CDR4 is well-posed for direct interaction with the MTX ligand. The five replaced residues were located in residues number 76 to 80 [3].

Based on the size of the binding pocket of Nb, cortisol already fits into the pocket. Hence, the substitution amino acid was selected to be the same size but more hydrophobic. Threonine 53 and serine 101 have the shortest distance with the ligand at approximately 3 Å. These polar residues should be in an h-bond interaction, but their orientation did not support the h-bond interaction. Besides, ligand and amino acid orientation are relatively meaningless in hydrophobic interaction. The interaction of antigen-antibody is mainly contributed by hydrophobic interaction [29]. As a result, we designed six mutants with single and double substitutions. Valine, isoleucine, and leucine are hydrophobic amino acids composed mostly of carbon and hydrogen, have very small dipole moments, and tend to be repelled from water. Threonine 53 and serine 101 are not exposed to the surface protein either. Hence substitution in this position will not disturb the overall structure. The size of replaced
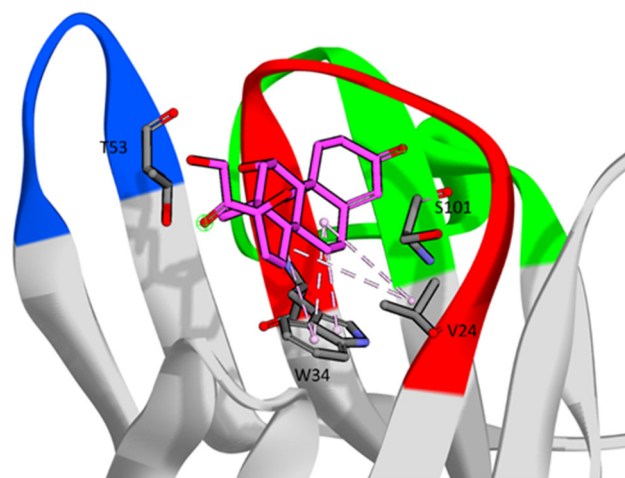
Fig 1. Initial interaction between Nb and cortisol. The red, blue, and green ribbons show the CDR1, CDR2, and CDR3, respectively. Cortisol is visualized in the pink stick, hydrophobic interaction in the pink dashed line, and residues around cortisol in the grey stick

amino acid is relatively not much different than previous. This was chosen to accommodate the ligand-binding pocket. Molecular docking and MD simulations were applied to evaluate and validate our design.

Modeling of Mutants

The mutant models were constructed from the WT structure. The crystal structure of Nb was resolved at good resolution, i.e., 1.57 Å. Because there were only one and/or two different amino acids, the identity of template and mutants was high.

The DOPE score, Ramachandran plot, and z-score were used to evaluate the quality of the mutants' model. According to the DOPE profile, all mutants have the same pattern as the template. Furthermore, the Ramachandran plot revealed that more than 90% of the residues in all mutants were located in the most favored regions, with no residues located in the disallowed region. A protein structure with more than 90% of its residues in the allowed region is classified as a good model [30]. In addition, the z-score of all mutants was equal to the quality of the structure source from X-ray and NMR (Fig. S1-S3).

Ligand Binding

To validate the methods, complex Nb-cortisol was

redocked. The binding energy was found to be -9.05 kcal/mol with an RMSD of 1.16 Å (Fig. 2). The low RMSD score (< 2Å) indicated that this pose was similar to the pose found in the crystal structure [31]. In contrast, the binding energy of all mutants varied in the score. MT1 and MT3 had higher affinity than WT with the binding energies of -9.12 and -9.87, respectively, compared to -9.05 kcal/mol. These mutants have CDR2 mutations. MT1 formed new hydrogen bonds with S30 and N77 and a new hydrophobic interaction with V53. While in MT3, a new hydrogen bond formed with S30 and K80 and a hydrophobic interaction with I53 (Fig. 3). It was indicated that our modification could generate new interactions.

MD simulations revealed that the WT, MT1, MT2, MT3, and MT5 are relatively stable, as evidenced by ligand snapshot every 20 ns and ligand's RMSD (Fig. 4). Furthermore, it showed that the ligand could maintain its conformation throughout the simulations. MT1 and MT3 also showed a stable RMSD, although a fluctuation was around 30–40 ns. Nonetheless, both systems can maintain the ligand's binding. Interestingly, MT5 showed stable movement although having the highest docking score than other mutants, -7.03 kcal/mol. The RMSD graph at around 40 ns indicates that almost all systems have a high deviation when viewed as a whole.

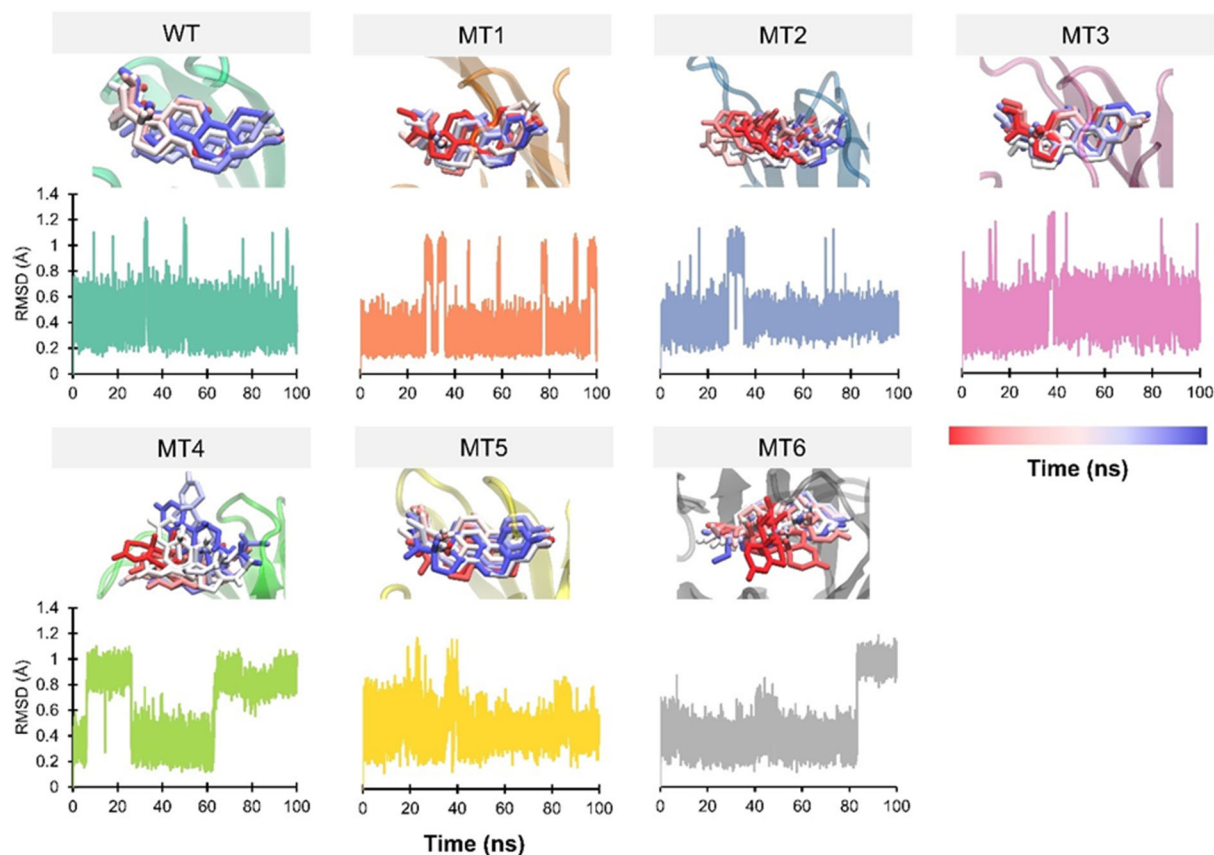The binding energy calculated from molecular docking and MD simulations revealed an interesting value. Although MT1 and MT3 have better binding affinity calculated from molecular docking, the affinity calculated from MD simulations showed differently. MT3, MT5, and MT6 were higher affinity than WT in MD simulations (Table 2). The Spearman's rank correlation coefficient of the binding energy from docking and MD simulation is -0.07. It revealed that there was no correlation between the value. Hence, it was suggested that MD simulations are necessary to evaluate the binding from molecular docking. Interestingly, after MD simulations, MT5 and MT6, which demonstrated lower binding affinity in molecular docking, have a higher affinity than WT. Nevertheless, the RMSD of the
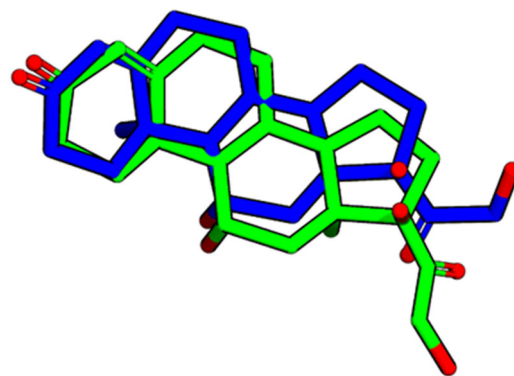
Fig 2. Superimpose of the docked pose (blue) and crystal structure (green)
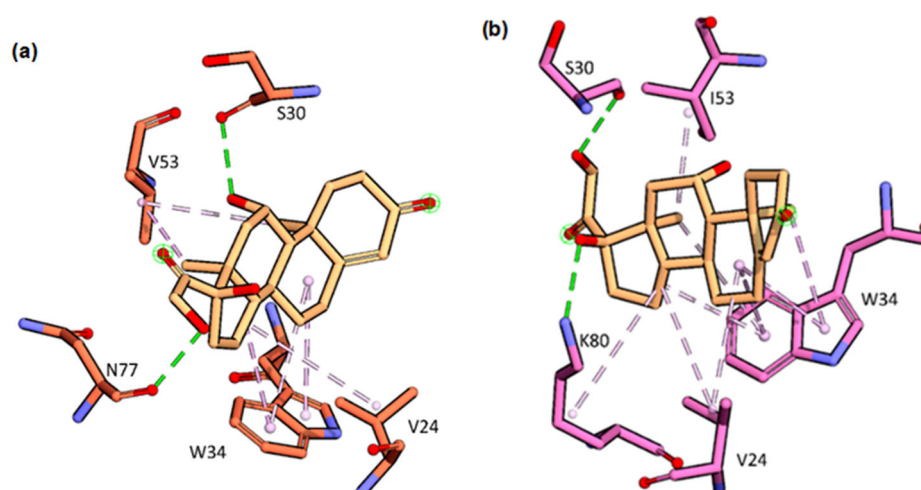
Fig 3. Interaction of cortisol and receptor in MT1 (a) and MT3 (b). Cortisol is represented in brown stick, the amino acid around ligand is shown in orange (MT1) and pink (MT3) stick, respectively, while the hydrogen bond and hydrophobic interaction are represented in green and pink dashed lines, respectively

Fig 4. Timestep evolution snapshot and RMSD of ligand every 20 ns throughout MD simulations

Table 2. Binding energy calculation from molecular docking and MD simulations
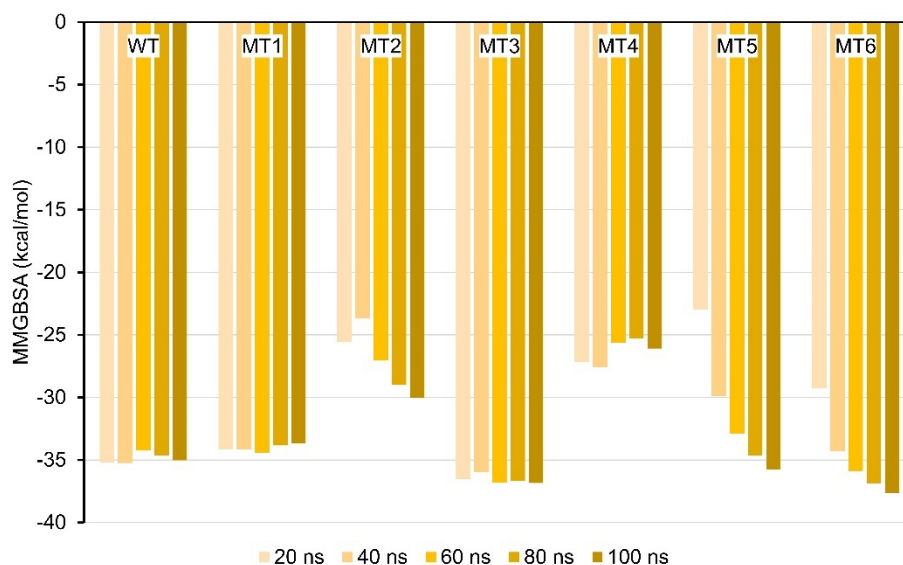
| System | Docking | MD Simulations | | | |
	Binding energy (kcal/mol)	Binding energy (kcal/mol)	Std. Deviation	Average RMSD receptor	Average RMSD ligand
WT	-9.05	-35.03	3.56	1.82	0.45
MT1	-9.12	-33.68	3.48	1.98	0.37
MT2	-8.99	-30.02	7.05	2.09	0.45
MT3	-9.87	-36.84	3.24	1.94	0.49
MT4	-8.51	-26.09	5.01	2.07	0.64
MT5	-7.03	-35.75	7.71	2.15	0.49
MT6	-8.44	-37.61	6.94	2.29	0.49

ligand in MT6 revealed the conformational changes at 80 ns indicating the ligand is unstable.

MMGBSA calculated every 20 ns cumulative, computed from a single trajectory every 1 ns, showed that MT3 has a stable value in the average of -36 kcal/mol and has a better value than WT, -35.03 kcal/mol, although at 100 ns MT6 has lower energy binding, -37.61 kcal/mol

(Fig. 5). A stable value implied that the ligand could bind to the receptor in a stable conformation required for ligand binding. In addition, a stable molecule indicates a fit interaction between the detected molecule with the capture molecule and is required for diagnostic purposes.

The intramolecular interaction was calculated from all systems showed differences in interaction from

Fig 5. Binding energy trajectory of cortisol bound receptor in every 20 ns cumulative

Table 3. Nonbonded interaction between cortisol and Nb reveal from molecular docking (D) and at the end of MD simulations

Interaction	WT		MT1		MT2		MT3		MT4		MT5		MT6	
	D	MD	D	MD	D	MD	D	MD	D	MD	D	MD	D	MD
H-Bond		1	2	2		2	2	2	6	3	6		6	3
Carbon H-bond		1				2		2				1	2	1
Alkyl	2	2	3	2	4	2	4	2	1		2	4	3	2
Pi-Alkyl	2	5	3	2	5	1	5	6	2	1		1	2	
Pi-sigma				1										

Note: in MD simulations, the nonbonded interaction was extracted from the last frame of MD trajectories

molecular docking and MD simulations. MT3, MT5, and MT6 were found to have better binding energy from MD simulations showed that there were only 2 hydrogen bonds occurred in MT3, 3 h-bond in MT6, and there was no h-bond occurred in MT5. In addition, hydrophobic interaction occurred the most in MT3. This hydrophobic interaction is described in the alkyl, pi-alkyl, and pi-sigma interaction. Besides, MT4, MT5, and MT6, which have the highest sum of H-bond in molecular docking, decreased interaction at the end of MD simulations (Table 3).

H-bond interaction from MD simulations is shown in Table 4. MT1, MT2, MT3, and MT6 showed longer h-bond occurrences than WT. Although MT4 has the largest number of interactions, it was not strong enough to keep the ligand in place when it only occurred for 1 ns. This finding is also in line with the RMSD of ligand that showed fluctuating value. Surprisingly, MT3, which

demonstrated the better binding energy from docking or MD, only has seven atoms that contribute to H-bond.

Nevertheless, this h-bond was occupied for 57 ns with S30, also occupied in WT for 45 ns. According to our findings, hydrophobic interaction donates a lot in the binding energy calculation. It is in line with the fact that hydrophobic interaction is the most common non-covalent interaction observed in protein-ligands from PDB [32]. In addition, VDW interaction energy calculated along MD simulations revealed that MT3 was lower than others (Table 5). This finding corresponded well to the interaction at the last frame of MD trajectories.

Structural Effect

The substitution made on the WT structure can alter the overall conformation. Therefore, we evaluate the

522

Indones. J. Chem., 2022, 22 (2), 515 - 525

Table 4. Hydrogen bond formation in Nb-cor complex throughout 100 ns of MD simulations

| System	Acceptor	Donor	Occ (ns)	System	Acceptor	Donor	Occ (ns)
WT	SER_30@O	HCY_127@O2	45	MT1	SER_30@O	HCY_127@O2	55
	HCY_127@O1	SER_101@OG	14		HCY_127@O4	ASN_77@ND2	16
	HCY_127@O4	ASN_77@ND2	6		ASN_77@OD1	HCY_127@O3	7
	HCY_127@O4	GLN_75@NE2	4		HCY_127@O4	GLN_75@NE2	6
	ASN_77@OD1	HCY_127@O3	2		HCY_127@O1	SER_101@OG	1
					HCY_127@O4	ASN_77@ND2	1
					ASN_77@OD1	HCY_127@O5	1
MT2	SER_30@O	HCY_127@O2	52	MT3	SER_30@O	HCY_127@O2	57
	SER_101@OG	HCY_127@O3	12		HCY_127@O4	ASN_77@ND2	12
	THR_28@O	HCY_127@O5	9		HCY_127@O4	GLN_75@NE2	8
	GLY_29@O	HCY_127@O2	7		ASN_77@OD1	HCY_127@O3	4
	HCY_127@O1	GLN_75@NE2	3		ASN_77@OD1	HCY_127@O5	3
	TYR_33@O	HCY_127@O3	3		HCY_127@O1	SER_101@OG	2
	GLY_29@O	HCY_127@O5	3		HCY_127@O3	THR_28@OG1	1
	ALA_54@O	HCY_127@O2	3				
MT4	HCY_127@O4	THR_28@N	23	MT5	SER_30@OG	HCY_127@O2	39
	GLY_32@O	HCY_127@O5	17		HCY_127@O5	GLY_29@N	25
	SER_30@O	HCY_127@O3	13		HCY_127@O1	GLN_75@NE2	22
	SER_30@O	HCY_127@O2	13		HCY_127@O2	SER_30@OG	12
	THR_28@OG1	HCY_127@O3	12		HCY_127@O5	THR_28@N	7
	THR_31@OG1	HCY_127@O2	10		ASN_77@OD1	HCY_127@O2	3
	HCY_127@O3	GLN_75@NE2	8		HCY_127@O2	ASN_77@ND2	2
	ASN_77@OD1	HCY_127@O3	7		THR_28@OG1	HCY_127@O3	2
	THR_28@OG1	HCY_127@O5	7		GLY_29@O	HCY_127@O3	1
	HCY_127@O5	THR_28@OG1	6		HCY_127@O1	THR_51@OG1	1
	HCY_127@O5	THR_53@OG1	6		VAL_24@O	HCY_127@O3	1
	THR_31@O	HCY_127@O5	5		HCY_127@O3	THR_28@N	1
	SER_30@O	HCY_127@O5	3				
	HCY_127@O5	THR_53@N	3	MT6	GLN_75@OE1	HCY_127@O3	60
	HCY_127@O4	GLY_29@N	3		HCY_127@O4	GLN_75@NE2	18
	HCY_127@O4	SER_30@N	2		ASN_77@OD1	HCY_127@O2	8
	HCY_127@O5	GLY_32@N	2		HCY_127@O4	ASN_77@ND2	7
	GLY_29@O	HCY_127@O2	1		ASN_77@OD1	HCY_127@O3	6
	THR_31@OG1	HCY_127@O3	1		GLN_75@OE1	HCY_127@O5	4
	HCY_127@O4	THR_28@OG1	1		HCY_127@O3	GLN_75@NE2	3
	TYR_33@O	HCY_127@O5	1		HCY_127@O4	ASN_77@ND2	3

structural effect to ensure that the protein's conformation remains unchanged. RMSD, RMSF, and radius of gyration (Rg) were calculated from all systems and showed a similar trend (Fig. 6). The RMSD graphic displayed an excellent value, which shows that all systems have a value lower than 2.5 Å. In contrast, the RMSF graphic revealed some high fluctuation in the same position across the entire system. The highest fluctuation

Table 5. VDW and electrostatic interaction calculated from MD simulations

System	VDW (kcal/mol)	Electrostatic (kcal/mol)
WT	-44.58	-16.55
MT1	-43.25	-17.29
MT2	-38.27	-17.88
MT3	-45.20	-17.85
MT4	-33.82	-15.16
MT5	-41.09	-17.79
MT6	-44.91	-18.56
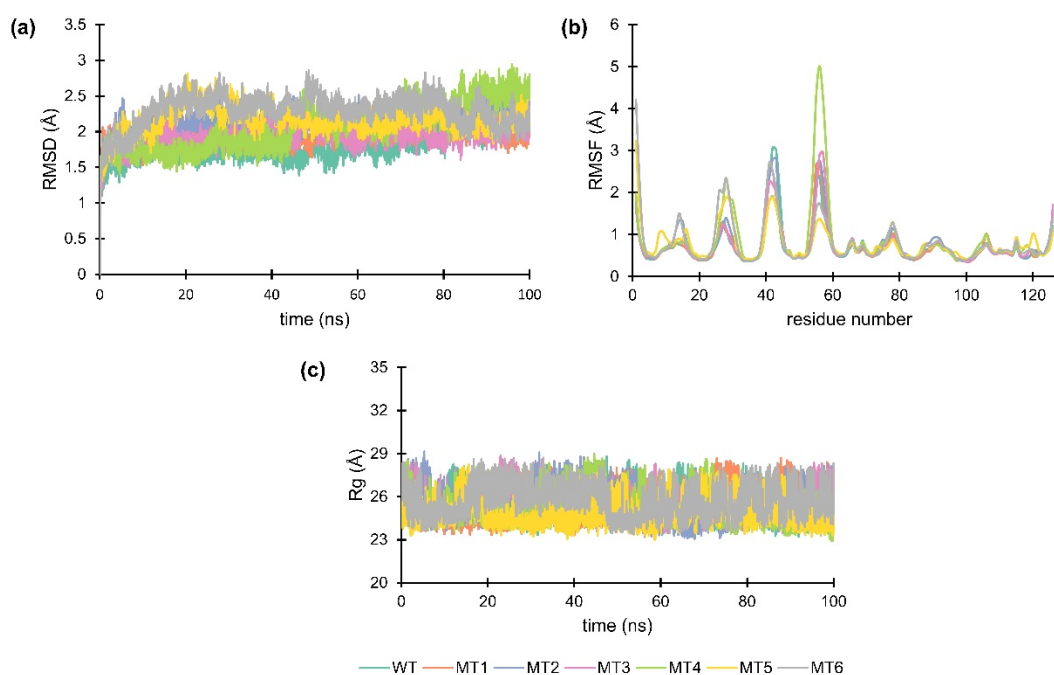
Fig 6. Profile of RMSD (A), RMSF (B), and radius of gyration (C) of receptor throughout 100 ns MD simulations, respectively

occurs around residues number 30, 40, and 60 ns which describe a flexible loop. Residue around 30 is the CDR1, a flexible loop to which the ligand bind, while residue around 40 is a loop located far from the ligand binding. Besides, the residues around 60 are the CDR2. The highest fluctuation in MT4 at residue was around 60 (CDR2), flexible loop, which corresponds to the ligand-binding, indicating that the ligand is not stable in MT4 and could not maintain its conformation. Other analyses showed that the Rg of all systems showed the same trend. Rg is defined as a protein's atom distribution around its axis [33]. All systems have a linear graph that indicates the compactness of protein structure throughout MD simulations. As a result, these findings implied that our

modification had no effect on the conformational structure but did affect ligand binding.

■ **CONCLUSION**

Increasing the affinity of Nb-cortisol is quite challenging. The CDR is the main area that contributes to the ligand binding. Because CDR1 plays an important in ligand binding, therefore our modification did not affect it. The addition of hydrophobic amino acids to CDR2 and CDR3 can improve the affinity, particularly at MT3, MT5, and MT6. Based on the docking energy, MM/GBSA energy, and ligand movement, MT3 has the highest binding affinity and is relatively more stable than others. The new hydrophobic interaction contributed to

the VDW energy calculation, which yielded the highest value compared to the others. It has been proposed that MT3 can increase the binding affinity of cortisol and is relatively stable. These results can guide the production of Nb in a recombinant laboratory.

■ ACKNOWLEDGMENTS

■ AUTHOR CONTRIBUTIONS

UB and NAS designed the experiments. UB conducted the experiment. UB, MY, NAS analyzed the data. UB, NAS, IM, DA, and MY wrote and revised the manuscript. All authors agreed to the final manuscript.

■ REFERENCES

[1] Hassanzadeh-Ghassabeh, G., Devoogdt, N., De Pauw, P., Vincke, C., and Muyldermans, S., 2013, Nanobodies and their potential applications, *Nanomedicine*, 8 (6), 1013–1026.

[2] Tabares-da Rosa, S., Wogulis, L.A., Wogulis, M.D., González-Sapienza, G., and Wilson, D.K., 2019, Structure and specificity of several triclocarban-binding single domain camelid antibody fragments, *J. Mol. Recognit.*, 32 (1), e2755.

[3] Fanning, S.W., and Horn, J.R., 2011, An anti-hapten camelid antibody reveals a cryptic binding site with significant energetic contributions from a nonhypervariable loop, *Protein Sci.*, 20 (7), 1196–1207.

[4] Huston, J.S., Levinson, D., Mudgett-Hunter, M., Tai, M.S., Novotný, J., Margolies, M.N., Ridge, R.J., Bruccoleri, R.E., Haber, E., Crea, R., and Oppermann, H., 1988, Protein engineering of antibody binding sites: Recovery of specific activity in an anti-digoxin single-chain Fv analogue produced in *Escherichia coli*, *Proc. Natl. Acad. Sci. U. S. A.*, 85 (16), 5879–5883.

[5] Rosano, G.L., and Ceccarelli, E.A., 2014, Recombinant protein expression in *Escherichia coli*: Advances and challenges, *Front. Microbiol.*, 5, 172.

[6] Löfblom, J., Frejd, F.Y., and Ståhl, S., 2011, Non-immunoglobulin based protein scaffolds, *Curr. Opin. Biotechnol.*, 22 (6), 843–848.

[7] Muyldermans, S., 2013, Nanobodies: Natural single-domain antibodies, *Annu. Rev. Biochem.*, 82 (1), 775–797.

[8] Bever, C.S., Dong, J.X., Vasylieva, N., Barnych, B., Cui, Y., Xu, Z.L., Hammock, B.D., and Gee, S.J., 2016, VHH antibodies: Emerging reagents for the analysis of environmental chemicals, *Anal. Bioanal. Chem.*, 408 (22), 5985–6002.

[9] Spinelli, S., Frenken, L.G.J., Hermans, P., Verrips, T., Brown, K., Tegoni, M., and Cambillau, C., 2000, Camelid heavy-chain variable domains provide efficient combining sites to haptens, *Biochemistry*, 39 (6), 1217–1222.

[10] Ding, L., Wang, Z., Zhong, P., Jiang, H., Zhao, Z., Zhang, Y., Ren, Z., and Ding, Y., 2019, Structural insights into the mechanism of single domain VHH antibody binding to cortisol, *FEBS Lett.*, 593 (11), 1248–1256.

[11] Corbalán-Tutau, D., Madrid, J.A., Nicolás, F., and Garaulet, M., 2014, Daily profile in two circadian markers "melatonin and cortisol" and associations with metabolic syndrome components, *Physiol. Behav.*, 123, 231–235.

[12] Pasha, S.K., Kaushik, A., Vasudev, A., Snipes, S.A., and Bhansali, S., 2014, Electrochemical immunosensing of saliva cortisol, *J. Electrochem. Soc.*, 161 (2), B3077.

[13] McEwen, B.S., 2002, Editorial: Cortisol, Cushing's syndrome, and a shrinking brain - New evidence for reversibility, *J. Clin. Endocrinol. Metab.*, 87 (5), 1947–1948.

[14] Kaushik, A., Vasudev, A., Arya, S.K., Pasha, S.K., and Bhansali, S., 2014, Recent advances in cortisol sensing technologies for point-of-care application, *Biosens. Bioelectron.*, 53, 499–512.

[15] Dalirirad, S., and Steckl, A.J., 2019, Aptamer-based lateral flow assay for point of care cortisol detection in sweat, *Sens. Actuators, B*, 283, 79–86.

[16] Dikme, O., and Dikme, O., 2019, Serum cortisol level as a useful predictor of surgical disease in

patients with acute abdominal pain, *Signa Vitae*, 15 (1), 27–31.

[17] le Roux, C.W., Chapman, G.A., Kong, W.M., Dhillo, W.S., Jones, J., and Alaghband-Zadeh, J., 2003, Free cortisol index is better than serum total cortisol in determining hypothalamic-pituitary-adrenal status in patients undergoing surgery, *J. Clin. Endocrinol. Metab.*, 88 (5), 2045–2048.

[18] Rice, P., Upasham, S., Jagannath, B., Manuel, R., Pali, M., and Prasad, S., 2019, CortiWatch: Watch-based cortisol tracker, *Future Sci. OA*, 5 (9), FSO416.

[19] Kaushik, A., Yndart, A., Jayant, R.D., Sagar, V., Atluri, V., Bhansali, S., and Nair, M., 2015, Electrochemical sensing method for point-of-care cortisol detection in human immunodeficiency virus-infected patients, *Int. J. Nanomedicine*, 10, 677–685.

[20] Frasconi, M., Mazzarino, M., Botrè, F., and Mazzei, F., 2009, Surface plasmon resonance immunosensor for cortisol and cortisone determination, *Anal. Bioanal. Chem.*, 394 (8), 2151–2159.

[21] Zainol Abidin, A.S., Rahim, R.A., Md Arshad, M.K., Fatin Nabilah, M.F., Voon, C.H., Tang, T.H., and Citartan, M., 2017, Current and potential developments of cortisol aptasensing towards point-of-care diagnostics (POTC), *Sensors*, 17 (5), 1180.

[22] Fiser, A., and Šali, A., 2003, MODELLER: Generation and refinement of homology-based protein structure models, *Methods Enzymol.*, 374, 461–491.

[23] Morris, G.M., Goodsell, D.S., Halliday, R.S., Huey, R., Hart, W.E., Belew, R.K., and Olson, A.J., 1998, Automated docking using a Lamarckian genetic algorithm and an empirical binding free energy function, *J. Comput. Chem.*, 19 (14), 1639–1662.

[24] Morris, G.M., Huey, R., Lindstrom, W., Sanner, M.F., Belew, R.K., Goodsell, D.S., and Olson, A.J., 2009, AutoDock4 and AutoDockTools4: Automated docking with selective receptor flexibility, *J. Comput. Chem.*, 30 (16), 2785–2791.

[25] Baroroh, U., Yusuf, M., Rachman, S.D., Ishmayana, S., Hasan, K., and Subroto, T., 2019, Molecular dynamics study to improve the substrate adsorption of *Saccharomycopsis fibuligera* R64 alpha-amylase by designing a new surface binding site, *Adv. Appl. Bioinf. Chem.*, 12, 1–13.

[26] Jakalian, A., Jack, D.B., and Bayly, C.I., 2002, Fast, efficient generation of high-quality atomic charges. AM1-BCC Model: II. Parameterization and validation, *J. Comput. Chem.*, 23 (16), 1623–1641.

[27] Wang, J., Wolf, R.M., Caldwell, J.W., Kollman, P.A., and Case, D.A., 2004, Development and testing of a general amber force field, *J. Comput. Chem.*, 25 (9), 1157–1174.

[28] Miller, B.R., Mcgee, T.D., Swails, J.M., Homeyer, N., Gohlke, H., and Roitberg, A.E., 2012, MMPBSA.py: An efficient program for end-state free energy calculations, *J. Chem. Theory Comput.*, 8 (9), 3314–3321.

[29] van Oss, C.J., Absolom, D.R., and Neumann, A.W., 1980, The "hydrophobic effect": Essentially a van der Waals interaction, *Colloid Polym. Sci.*, 258 (4), 424–427.

[30] Laskowski, R., MacArthur, M., Moss, D., and Thornton, J., 1993, PROCHECK: A program to check the stereochemical quality of protein structures, *J. Appl. Crystallogr.*, 26 (2), 283–291.

[31] Hernández-Santoyo, A., Tenorio-Barajas, A.Y., Altuzar, V., Vivanco-Cid, H., and Mendoza-Barrera, C., 2013, "Protein-Protein and Protein-Ligand Docking" in *Protein Engineering: Technology and Application*, Eds. Tomohisa Ogawa, T., IntechOpen, London, 21.

[32] de Freitas, R.F., and Schapira, M., 2017, A systematic analysis of atomic protein-ligand interactions in the PDB, *MedChemComm*, 8 (10), 1970–1981.

[33] Sneha, P., and Priya Doss, C.G., 2016, Molecular dynamics: New frontier in personalized medicine, *Adv. Protein Chem. Struct. Biol.*, 102, 181–224.